Florian Zikeli, Vittorio Vinciguerra, Anna Rita Taddei, Alessandro D'Annibale, Manuela Romagnoli and Giuseppe Scarascia Mugnozza*

Isolation and characterization of lignin from beech wood and chestnut sawdust for the preparation of lignin nanoparticles (LNPs) from wood industry side-streams

https://doi.org/10.1515/hf-2017-0208
Received December 15, 2017; accepted May 25, 2018; previously published online xx

Abstract: Lignin was isolated through mild acidolysis from local wood sources such as beech wood and chestnut wood sawdust, a high-volume side product of wood industries. The lignin fractions were characterized by pyrolysis-gas chromatography/mass spectrometry (Py-GC/MS), Fourier-transform infrared (FTIR), ultraviolet-visible (UV-Vis) and two-dimensional heteronuclear single-quantum correlation nuclear magnetic resonance (2D HSQC NMR) spectroscopies and size exclusion chromatography (SEC). The Klason lignin (KL) content and polysaccharide composition were determined using traditional methods. Lignin nanoparticles (LNPs) were prepared *via* a non-solvent method involving dialysis and characterized by scanning electron microscopy (SEM) and transmission electron microscopy (TEM) and FTIR and UV-VIS spectroscopies. Semi-porous as well as hollow nanoparticles endowed with a spherical shape were observed. The large majority of the LNPs exhibited an average particle diameter of 90–120 nm. Dynamic light scattering (DLS) analysis showed that both distribution and frequency of dimensional classes of LNPs are clearly affected by the lignin solvent system, i.e. solvent selection governs the size distribution of LNPs.

Keywords: beech, chestnut, dynamic light scattering (DLS), FTIR, lignin nanoparticles (LNPs), NMR, pyrolysis-GC/MS, SEM

***Corresponding author: Giuseppe Scarascia Mugnozza,** Università degli Studi della Tuscia, Department for Innovation in Biological Systems, Food and Forestry, Via San Camillo de Lellis, snc, 01100 Viterbo, Italy, Phone: +39 0761 35758, e-mail: gscaras@unitus.it
Florian Zikeli, Vittorio Vinciguerra, Alessandro D'Annibale and Manuela Romagnoli: Università degli Studi della Tuscia, Department for Innovation in Biological Systems, Food and Forestry, Via San Camillo de Lellis, snc, 01100 Viterbo, Italy
Anna Rita Taddei: Università degli Studi della Tuscia, Great Equipment Center, Section of Electron Microscopy, Largo dell'Università snc, 01100 Viterbo, Italy

Introduction

Lignin *in planta* acts as a natural protective agent against bacterial or fungal attack as well as against weathering, rendering the cell walls waterproof. Technical lignin is not only a by-product of the pulping industry, but also a side-stream of the second generation ethanol biorefineries. Lignin valorization is essential for the development of biorefinery concepts as a part of integrated forestry and wood industries (Ragauskas et al. 2014; Mattsson et al. 2017). The conversion of waste into value-added products is listed within the three structural pillars of the EU Bioeconomy Strategy (Paletto et al. 2017).

Beech wood is produced in high amounts and has many applications (Houston Durrant et al. 2016), in the course of which huge amounts of waste are generated. The same applies to chestnut wood, which is essential for barrel and railway sleeper production (Conedera et al. 2016). Currently, wood wastes are mainly burned for energy generation with revenues around €26 per ton of wood biomass (Russo et al. 2016) and utilizations with more added value are sought. Lignin is the only natural feedstock for aromatic compounds (Tuck et al. 2012). Lignin isolation from wood wastes like sawdust and the development of high-value lignin applications would create new value chains and contribute to a circular-economy concept.

As a new promising application, lignin nanoparticles (LNPs) were synthesized by taking advantage of its hydrophobicity and tendency for self-aggregation in the presence of water. Different synthesis routes and new applications of LNPs as antimicrobial and ultraviolet (UV)-protective agents, antioxidants, metal-ion sorbents or as reinforcement elements in polymeric nanocomposites have been recently reviewed in detail (Fortunati et al. 2016; Ago et al. 2017; Beisl et al. 2017). Within the field of nanoparticle-based applications, lignin is a very promising candidate to compete with synthetic or inorganic materials due to its advantages, such as low toxicity, biodegradability, low cost and high availability (Ago et al. 2017).

The objective of this study was to assess the suitability of industrial wastes of beech and chestnut woods for LNP production. Acidolysis lignin (AL) fractions were isolated

and structurally characterized by a combination of pyrolysis-gas chromatography/mass spectrometry (Py-GC/MS) and heteronuclear single-quantum correlation nuclear magnetic resonance (HSQC NMR) spectroscopy. For LNP production, the "anti-solvent procedure" was applied, which is based on particle formation *via* the introduction of water as an anti-solvent in the starting lignin solution.

Materials and methods

Beech wood (*Fagus sylvatica* L.) and sawdust from sweet chestnut wood (*Castanea sativa* Mill.) from the Cimini Mountains in Lazio region, Italy (Piangoli Legno SNC, Soriano nel Cimino, VT, Italy), were air-dried and then cut to pass through a 35-mesh sieve in an IKA MF 10.1 cutting mill (IKA®-Werke GmbH & Co. KG, Staufen, Germany). The milled wood was then Soxhlet-extracted for 15 h with acetone (Sigma-Aldrich, Milan, Italy) and dried at room temperature. 1,4-Dioxane (Alfa Aesar, ACS grade 99+%) was from Thermo Fisher (Kandel) GmbH (Karlsruhe, Germany). American Chemical Society (ACS)-grade NaOH and dimethyl sulfoxide (DMSO) (>99.9%) were from Carlo Erba reagents (Milan, Italy) and Sigma-Aldrich (Milan, Italy), respectively.

Lignin extraction: The milled and acetone-extracted wood samples were treated according to a modified protocol by Gellerstedt et al. (1994) to produce AL. The sample was heated under reflux in 0.1 M HCl in dioxane/water 82:18 (v/v) for 2 h. After separation of the solid wood residue by filtration and subsequent washing with dioxane/water, the solvent in the lignin-containing filtrate was removed under reduced pressure in a rotary evaporator. Concomitantly, small aliquots of water were added for precipitating the water-insoluble lignin and to avoid an increase in the acidity of the mixture that might promote lignin condensation reactions. The precipitated AL was filtered using a Whatman filter paper no. 4 (Sigma-Aldrich, Milan, Italy), washed with water until a neutral pH was obtained and dried over P_2O_5 under vacuum in a desiccator.

Preparation of lignin nanoparticles (LNPs): The modified protocol by Frangville et al. (2012) was applied, which is based on the introduction of water as an anti-solvent into the initial lignin solution via dialysis tubes made of regenerated cellulose with a molecular weight cut-off of 6–8 kDa (SpectraPor® 1 Dialysis Membrane Standard RC Tubing, 6–8 kDa, Spectrum Labs, CA, USA). The initial lignin solution was prepared by NaOH (10 mM in water), dioxane/water 82:18 (v:v) and DMSO and the solutions were dialyzed (1:400 ratio) against Milli-Q water, which was replaced twice, in a 4-l beaker for 48 h under magnetic stirring. The resulting LNP dispersions were recovered and kept in the fridge.

It is noteworthy that the lignin solvents employed in this study (i.e. dioxane/water, DMSO and 10 mM NaOH) were selected on the basis of their lower toxicity than the generally used tetrahydrofuran (THF) (Lievonen et al. 2016; Xiong et al. 2017a,b). Li et al. (2016) also dissolved kraft lignin in dioxane/water for subsequent nanosphere preparation. Of course, dioxane/water (82:18) is also toxic and should not be inhaled. DMSO is a highly biocompatible solvent and its recovery from aqueous media is possible (Sundergopal et al. 2011; Nalaparaju and Jiang 2012; Zajáros and Matolcsy 2016), and thus its application in industrial scale is possible.

Chemical composition: Extractive contents of the different wood species were determined gravimetrically after acetone extraction for 15 h in a Soxhlet apparatus. The Klason lignin (KL), cellulose and hemicellulose contents of wood were determined according to TAPPI T 222 om-02, Van Soest (1963) and Van Soest and Wine (1967), respectively.

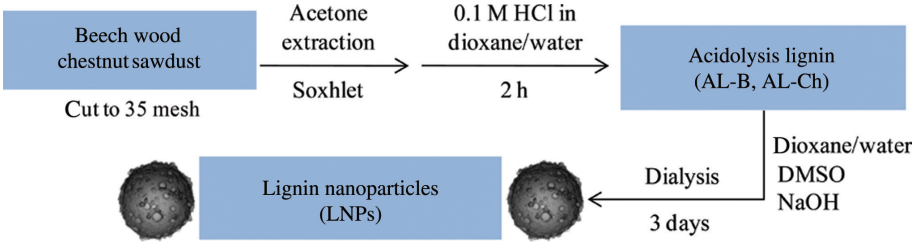

Scheme 1: Isolation procedure for acidolysis lignin (AL) fractions from beech wood and chestnut sawdust (AL-B, AL-Ch) and eventual preparation of lignin nanoparticles (LNPs).

Table 1: Extractives and Klason lignin contents of beech and chestnut wood samples, the acidolysis lignins (AL-B, AL-Ch) and the acidolysis residues (ResB, ResCh).

Sample	Extractives[a] (%)	Klason lignin (%)	Cellulose (%)	Hemicellul. (%)	M_w (Da)	M_n (Da)	M_w/M_n	Yield (%)
Beech	2.0	28.4	37.0	24.8	–	–	–	–
ResB	–	21.2	63.0	6.6	–	–	–	–
AL-B	–	81.2	–	–	23 990	4380	5.5	25.4
Chestnut	6.6	33.1	32.7	18.2	–	–	–	–
ResCh	–	22.8	62.0	5.6	–	–	–	–
AL-Ch	–	79.7	–	–	13 000	2820	4.6	31.1

[a]Acetone.

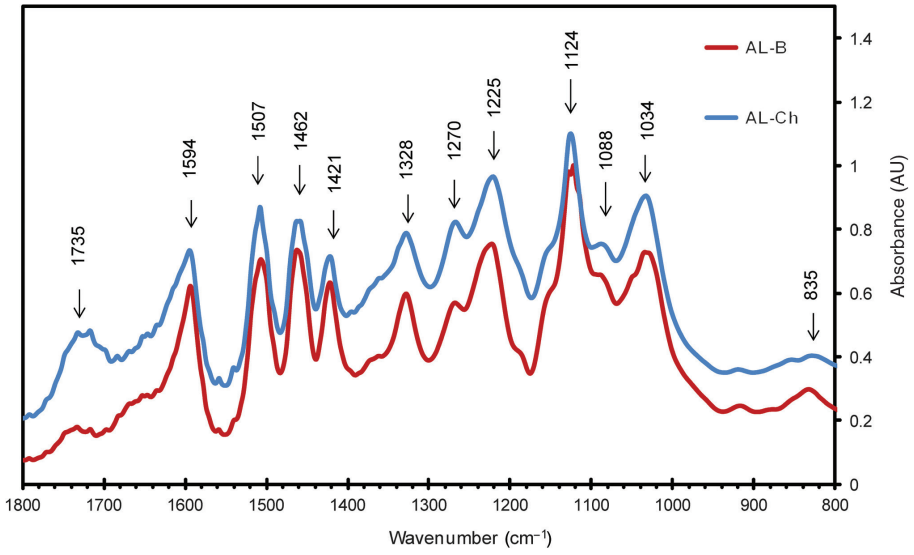

Figure 1: FTIR spectra of the isolated acidolysis lignin (AL) fractions from beech wood (AL-B) and chestnut sawdust (AL-Ch).

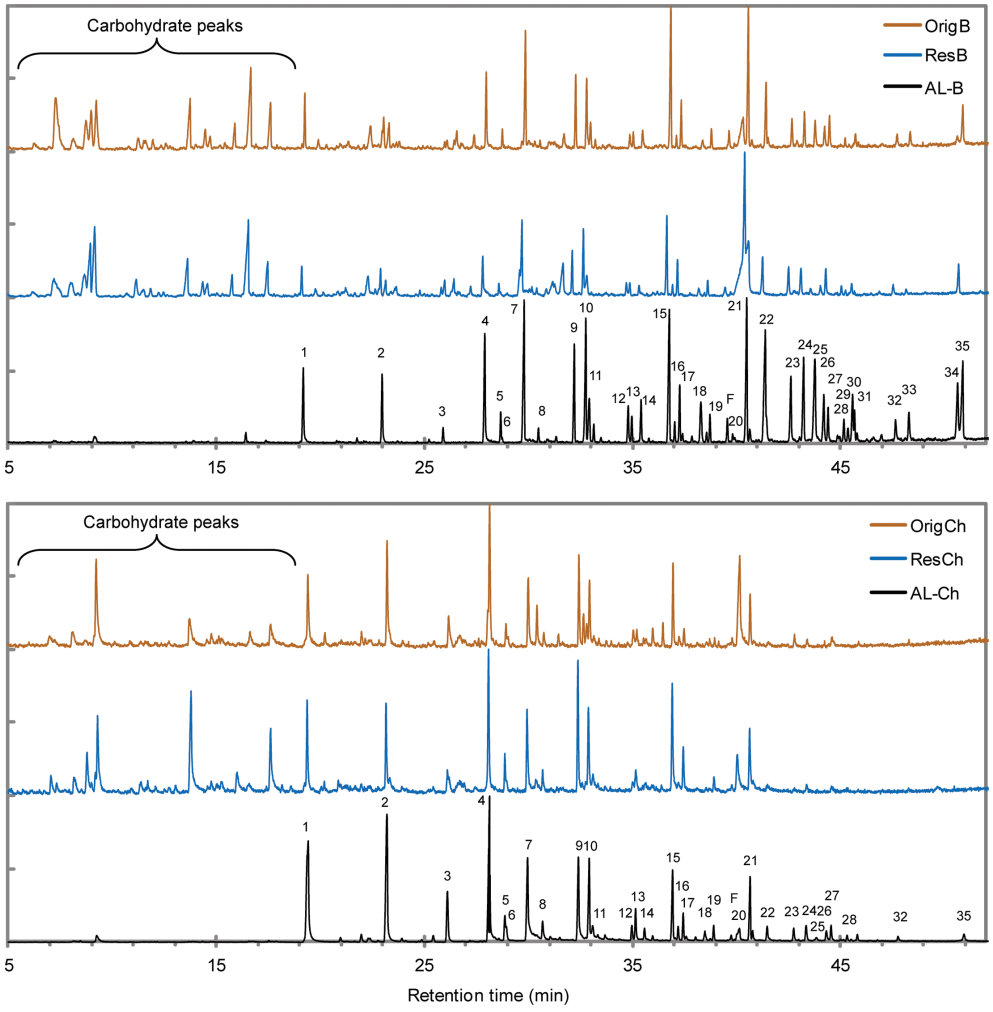

Figure 2: Pyrograms of acidolysis lignin (AL) of beech wood and chestnut sawdust (AL-B, AL-Ch), original beech wood and chestnut sawdust (OrigB, OrigCh) and the respective acidolysis residues (ResB, ResCh).

FTIR and UV-VIS spectroscopy: The FTIR spectra were recorded using a Jasco FTIR-4100 instrument (KBr technique, 4 cm^{-1} resolution). The pellets had a lignin concentration of 2% (wt.); Specac minipellets press (Specac Inc., Fort WA, USA) was applied. The UV-VIS spectra of the AL and LNP fractions in Milli-Q water, which served as blank, were recorded on a Jasco V-630 spectrophotometer (Jasco Corporation, MD, USA).

Analytical pyrolysis (Py-GC/MS): Pellets of fine-powdered wood, lignin and acidolysis residues (1.5–2 mg) were pressed in a special syringe and eventually directly pyrolyzed at 450°C in a Pyrojector II (SGE Analytical Science, Trajan Scientific and Medical, Victoria, Australia) microfurnace Py chamber. Py products were separated in a HP 5890 Series II Plus gas chromatograph (Agilent Technologies, CA, USA) endowed with a Restek Rtx®-1701 (30 m × 0.25 mm i.d.) capillary column (Restek Corporation, PA, USA). Helium was the carrier gas at a pressure of 100 kPa in the pyrolyzer and 70 kPa in the GC injector (280°C, 1:20 split ratio). The temperature in the oven was held initially at 45°C for 4 min, then increased to 240°C at a heating rate of 4°C min^{-1} and finally until 280°C at a rate of 39°C min^{-1}. A HP 5971A-MSD mass spectrometer (Agilent Technologies, CA, USA) was used in the electron ionization (EI) mode at 70 eV and scans from m/z 35 to

Table 2: Retention times, relative abundances, assignment to guaiacyl-type (G) or syringyl-type (S) aromatic subunits of pyrolysis products of original beech wood (OrigB), original chestnut sawdust (OrigCh), the respective isolated acidolysis lignin fractions (AL-B, AL-Ch) and the acidolysis residues (ResB, ResCh) and their respective S/G ratios.

				Beech			Chestnut		
#	Pyrolysis product	Origin	RT (min)	OrigB (%)	AL-B (%)	ResB (%)	OrigCh (%)	AL-Ch (%)	ResCh (%)
1				3.7	3.4	3.0	7.4	11.8	5.1
2	4-Methylguaiacol	G	23.19	2.3	3.0	3.1	7.7	11.1	4.2
3	4-Ethylguaiacol	G	26.10	0.4	0.6	1.1	3.1	3.8	1.1
4	4-Vinylguaiacol	G	28.12	5.4	4.8	4.7	9.6	11.7	8.2
5	Eugenol	G	28.85	1.2	0.9	1.0	0.9	1.6	2.3
6	4-Propylguaiacol	G	28.92	0.1	0.1	0.2	0.0	0.9	0.0
7	Syringol	S	29.95	8.7	6.6	8.1	5.0	7.4	5.2
8	Isoeugenol (*cis*)	G	30.67	0.4	0.5	0.5	1.0	1.6	1.3
9	Isoeugenol (*trans*)	G	32.39	5.1	3.9	4.4	5.4	6.4	6.5
10	4-Methylsyringol	S	32.91	5.5	5.6	7.2	3.8	5.3	4.5
11	Vanillin	G	33.07	2.1	2.6	3.8	0.0	1.5	1.1
12	Homovanillin	G	34.96	1.1	1.6	1.6	1.4	1.0	0.0
13	4-Ethylsyringol	S	35.14	1.1	1.0	1.6	1.3	1.9	1.5
14	Acetoguaiacone	G	35.57	1.5	1.7	1.0	0.5	1.0	0.0
15	4-Vinylsyringol	S	36.91	10.6	6.6	8.9	4.8	4.2	6.2
16	Guaiacylacetone	G	37.18	0.7	0.8	1.0	0.6	0.7	0.0
17	4-Allylsyringol	S	37.42	2.9	2.1	3.5	0.9	1.4	2.4
18	Coniferyl alcohol (*cis*)	G	38.46	0.9	2.6	1.1	0.0	0.8	0.0
19	4-Propenylsyringol (*cis*)	S	38.88	1.3	1.1	1.8	0.5	0.9	0.9
F	$C_{11}H_{12}O_3$[a]		39.73	1.9	1.3	1.7	1.2	0.4	1.1
20	Levoglucosane	PS	40.13	5.5	0.3	n.d.	11.0	1.7	3.4
21	4-Propenylsyringol (*trans*)	S	40.64	11.2	6.8	13.2	3.1	3.7	3.0
22	Syringaldehyde	S	41.46	4.8	7.7	5.1	0.0	1.3	0.0
23	Homosyringaldehyde	S	42.73	2.3	3.1	3.8	0.8	1.0	0.0
24	Acetosyringone	S	43.32	2.8	4.1	3.6	0.6	1.2	0.0
25	Coniferyl alcohol (*trans*)	G	43.70	2.5	5.6	0.9	0.0	0.1	0.0
26	Coniferaldehyde	G	44.31	1.7	2.4	1.4	0.0	0.8	0.0
27	Syringylacetone	S	44.53	2.3	1.4	2.9	0.9	1.1	0.0
28	Propiosyringone	S	45.30	0.6	1.0	1.1	0.0	0.4	0.0
29	Propiosyringone, α-oxy-	S	45.95	0.2	0.6	0.6	0.0	0.0	0.0
30	4-Oxy-allylsyringol	S	46.19	0.2	2.2	0.0	0.0	0.0	0.0
31	Sinapyl alcohol (*isomer*)	S	46.27	1.0	1.1	1.4	0.0	0.0	0.0
32	Dihydrosinapyl alcohol	S	47.74	1.3	1.2	1.2	0.0	0.3	0.0
33	Sinapyl alcohol (*cis*)	S	48.79	1.4	1.4	0.9	0.0	0.0	0.0
34	Sinapyl alcohol (*trans*)	S	51.23	0.8	3.8	0.0	0.0	0.0	0.0
35	Sinapaldehyde	S	50.91	4.0	5.0	4.0	0.0	0.6	0.0
	S/G ratio			2.16	1.81	2.39	0.58	0.56	0.74
	S/G ratio corrected[b]			0.80	0.78	0.94	0.10	0.19	0.11

PS indicates polysaccharides' origin. [a]Compounds no. 65 and 66 in Faix et al. (1990a).
[b]Corrected S_{Lignin} (%) = $-5.9 + 0.704 \times S_{\%Py}$ (Choi et al. 2001).

m/z 500 were run in 0.7 s cycles. Py products were identified by mass spectra interpretation and by comparison with National Institute of Standards and Technology (NIST) and Wiley computer libraries and the literature (Faix et al. 1990a,b, 1991a,b). For each pyrogram, the relative area of 34 principal phenolic Py products was calculated, compared to the most intense peak and grouped as guaiacyl-type (G-type) or syringyl-type (S-type) lignin fragments and the S/G ratio was calculated under consideration of a correction factor according to Choi et al. (2001). Py experiments were conducted in duplicate and the relative areas of the pyrograms were averaged.

Two-dimensional (2D) HSQC NMR spectroscopy: The spectra were recorded from 70 mg lignin samples in 700 µl DMSO-d_6 on a Bruker AVANCE III 400 MHz spectrometer (Bruker UK Limited, Coventry, UK) equipped with gradient probe (90 scans). The Bruker standard pulse program "hsqcetgpsi" was applied with spectral widths of 12.5 ppm and 157 ppm in the ^{1}H- and ^{13}C-dimensions, respectively. Data processing was performed using Bruker TopSpin software. For a semi-quantitative analysis, the integrals of the HSQC cross-peaks were determined and compared by means of the MestReNova v6.0.2 software (Mestrelab Research S.L., Santiago di Compostela, Spain). Signal assignment was done according to literature (Ralph et al. 2009; Kim and Ralph 2010; Lourenço et al. 2016; Chen et al. 2017). The monomeric ratio of the AL fractions was estimated from the C_2-H_2 correlations from S, G and H lignin units in the aromatic region of the HSQC spectra. The C_α-H_α correlations served for the evaluation of the relative abundances of the different lignin inter-unit linkages as well as the ratio of cinnamyl aldehyde end-groups.

Molar mass distribution (MMD): High-performance size exclusion chromatography (HP-SEC) analysis was performed on a Varian HPLC system with UV detection (280 nm) in 10 mM NaOH solution with 20 mM $NaNO_3$. The details are as follows: PSS MCX column with a particle size of 5 µm and a pore size of 1000 Å (PSS Polymer Standard Services, Mainz, Germany); flow rate 0.6 ml min^{-1}. The concentration of the lignin samples and the injection volume were 3 mg ml^{-1} and

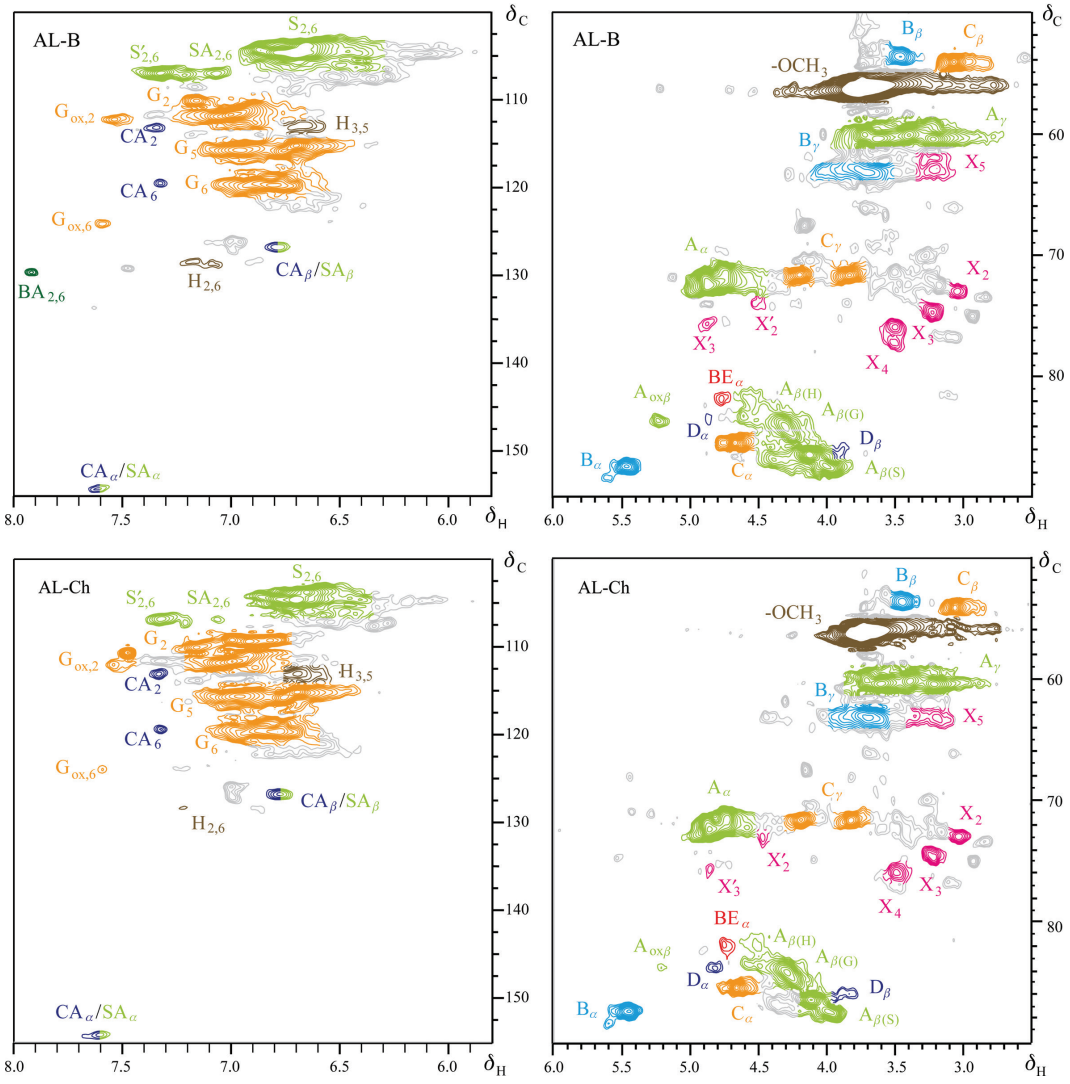

Figure 3: Two-dimensional HSQC NMR spectra of the acidolysis lignins (ALs) from beech wood and chestnut sawdust (AL-B, AL-Ch). Left side: aromatic regions; right side: oxygenated side-chain regions. For chemical structures and respective NMR shifts see Figure 4 and Table 4.

Table 3: Signal assignments of the ^{13}C-^{1}H correlation peaks in the 2D HSQC NMR spectra of the isolated wheat straw lignin fractions, according to Chen et al. (2017), Kim and Ralph (2010), Lourenço et al. (2016) and Ralph et al. (2009).

δ_C/δ_H (ppm)	Assignment (label)
53.6/3.45	C_β-H_β in phenylcoumaran β-5′ substructures (**B_β**)
54.0/3.04	C_β-H_β in resinol substructures β-β′ (**C_β**)
60.0/ 2.90–3.90	C_γ-H_γ in γ-hydroxylated β-O-4′ substructures (**A_γ**)
63.0/3.19	C_5-H_5 in β-D-xylopyranoside (**X_5**)
63.3/3.75	C_γ-H_γ in phenylcoumaran β-5′ substructures (**B_γ**)
71.6/ 3.83 + 4.20	C_γ-H_γ in resinol substructures β-β′ (**C_γ**)
72.3/4.77	C_α-H_α in β-O-4′ substructures (**A_α**) linked to a G unit
73.1/3.03	C_2-H_2 in β-D-xylopyranoside (**X_2**)
74.1/4.50	C_2-H_2 in 2-O-acetyl-β-D-xylopyranoside (**X'_2**)
74.7/3.22	C_3-H_3 in β-D-xylopyranoside (**X_3**)
75.8/4.87	C_3-H_3 in 3-O-acetyl-β-D-xylopyranoside (**X'_3**)
76.6/3.49	C_4-H_4 in β-D-xylopyranoside (**X_4**)
81.8/4.76	C_α-H_α in benzyl ether substructures (**BE_α**)
82.7/4.55	C_β-H_β in β-O-4′ substructures (**$A_{\beta(H)}$**) linked to a H unit
83.7/4.82	C_α-H_α in dibenzodioxocin substructures (**D_α**)
83.7/5.21	C_β-H_β in α-oxidized (C_α=O) β-O-4′ substructures (**$A_{ox\beta}$**)
84.3/4.29	C_β-H_β in β-O-4′ substructures (**$A_{\beta(G)}$**) linked to a G unit
85.6/4.66	C_α-H_α in resinol β-β′ substructures (**C_α**)
85.9/3.84	C_β-H_β in dibenzodioxocin substructures (**D_β**)
87.1/4.04	C_β-H_β in β-O-4′ substructures (**$A_{\beta(S)}$**) linked to a S unit
87.9/5.50	C_α-H_α in phenylcoumaran β-5′ substructures (**B_α**)
104.5/6.63	$C_{2,6}$-$H_{2,6}$ in syringyl units (**$S_{2,6}$**)
106.8/7.06	$C_{2,6}$-$H_{2,6}$ in sinapaldehyde units (**$SA_{2,6}$**)
107.0/7.28	$C_{2,6}$-$H_{2,6}$ in α-oxidized (C_α=O) syringyl units (**$S'_{2,6}$**)
110.5/6.97	C_2-H_2 in guaiacyl units (**G_2**)
111.2/7.50	C_2-H_2 in oxidized guaiacyl units (**G'_2**)
111.6/7.31	C_2-H_2 in coniferaldehyde (**CA_2**)
115.9/ 6.95 + 6.70	C_5-H_5 and C_6-H_6 in guaiacyl units (**G_5, G_6**)
119.1/6.84	C_6-H_6 in guaiacyl units (**G_5, G_6**)
111.6/7.31	C_2-H_2 in coniferaldehyde units (**CA_2**)
119.4/7.32	C_6-H_6 in oxidized guaiacyl units (**G'_6**)
126.7/6.78	C_β-H_β in cinnamyl aldehyde end groups (**CA_β**)
128.9/7.20	$C_{2,6}$-$H_{2,6}$ in *p*-hydroxyphenyl units (**$H_{2,6}$**)
129.6/7.91	$C_{2,6}$-$H_{2,6}$ in *p*-hydroxybenzoic acid/aldehyde (**$BA_{2,6}$**)
154.2/7.60	C_α-H_α in cinnamyl aldehyde end groups (**CA_α, SA_α**)

10 µl, respectively. Calibration for molar mass (MM) determination was done using sodium polystyrene sulfonate reference standards (PSS Polymer Standard Services, Mainz, Germany) with the MMs at peak maximum (M_p): 65 400, 33 500, 15 800, 6430, 1670, 891 and 208 Da. Particle size of the aqueous LNP suspensions was determined by dynamic light scattering (DLS) on a Malvern Zetasizer Nano ZS instrument (Malvern Instruments Ltd, UK).

SEM and TEM of LNP dispersions: Drops of the LNP suspensions were adsorbed onto a polylysinated glass coverslip and air dried at 25°C. The holders were attached to aluminum stubs by a carbon tape and the samples were sputter-coated with gold in a Balzers MED 010 unit (Oerlikon Balzers, Balzers, Liechtenstein). A JEOL JSM 6010LA SEM was applied (JEOL Limited, Tokyo, Japan). For TEM analysis, 10 µl of the LNP suspensions were adsorbed onto 200-mesh Formvar-carbon coated copper grids for 5 min. Excess liquid was removed by gently touching the grid with a filter paper. For negative staining, the specimen grid was first washed with a drop of 2% uranyl acetate in distilled water followed by repetition of this step once more, in the course of which the specimen grid is floated for 90 s on a new drop of negative staining solution. Instruments used: A JEOL 1200 EX II electron microscope (100 kV) and micrographs were acquired with an Olympus SIS VELETA CCD camera (Olympus Soft Imaging Solutions GmbH, Münster, Germany) equipped with iTEM software (EMSIS GmbH, Münster, Germany).

Results and discussion

Isolation and general structural characteristics of ALs

The isolation scheme was aimed at obtaining lignin fractions with a high purity, while preserving the structural properties of native lignins (Scheme 1). Mild acidolysis seems to be a reasonable compromise to produce lignin with a high purity, high isolation yield and methodological investment in terms of chemical consumption and working time. According to Gellerstedt et al. (1994), mild acidolysis delivers pure lignin fractions with little polysaccharide residues, but condensation reactions or cleavage of α- and β-ether linkages may occur under acidic conditions. Our recent works showed that the ratio of β-O-4′ substructures in AL fractions remained high and thus cleavage of lignin chemical bonds is kept within low limits (Zikeli et al. 2014, 2016). The isolated lignin fractions from beech and chestnut woods (AL-B, AL-Ch) resulted in KL contents around 80% and their recovery yields were higher than 25%, based on the KL content of the original wood samples (Table 1). Very low hemicellulose and high cellulose contents were found in the acidolysis residues (ResB and ResCh), which is indicative of a specific dissolution of hemicelluloses. The FTIR spectra (Figure 1) confirmed the high KL content, as no bands could be solely attributed to polysaccharides (897, 985, 1058, and 1163 cm^{-1}). The presence of minor carbohydrate impurities was indicated by the bands at 1371 and 1733 cm^{-1}. Detailed band assignments are published in the literature (Faix 1992; Colom et al. 2003; Traoré et al. 2016; Moghaddam et al. 2017). Based on the IR band intensities, it is obvious that beech lignin contains more S units than chestnut lignin, i.e. in beech lignin $I_{1462} > I_{1507}$, whereas in chestnut lignin $I_{1462} < I_{1507}$. Moreover, the band at 1270 cm^{-1} (a typical G band) of chestnut lignin is more pronounced than in the case of beech lignin (Faix 1991).

Much higher MM averages were found for beech lignin than chestnut lignin (Table 1). Beech AL showed

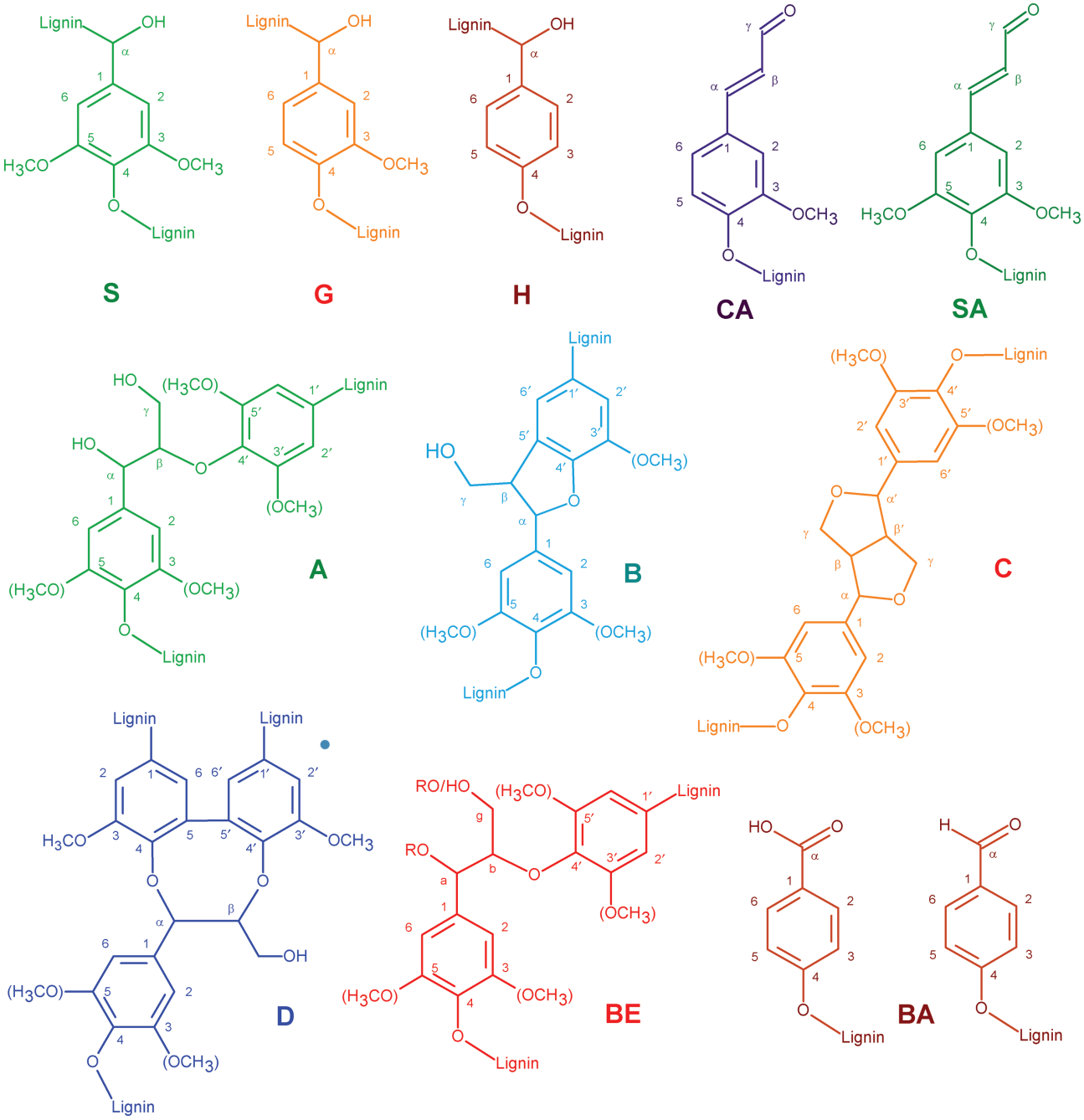

Figure 4: Lignin structural elements related to the respective HSQC cross-signals in the NMR spectra: (S) syringyl units, (G) guaiacyl units, (H) *p*-hydroxyphenyl units, (CA) coniferyl aldehyde units, (SA) sinapaldehyde units, (A) β-O-4′ substructures, (B) phenylcoumaran β-5′ substructures, (C) resinol β-β′ substructures, (D) dibenzodioxocin substructures, (BE) benzyl ether substructures, (BA) *p*-hydroxybenzoic acid/aldehyde substructures.

Table 4: Monomeric compositions and ratios of different inter-unit linkages of the acidolysis lignin (AL) fractions from beech wood and chestnut sawdust (AL-B, AL-Ch).

	Monomeric units (%)				Interunit linkages (%)					
Lignin fraction	**S units**	**G units**	**H units**	**S/G ratio**	**β-O-4′**	**β-5′**	**β-β′**	**Bzl-ether**	**DBDO**	**CA end-group**
AL-B	62	37	1	1.68	83	7	8	2	<1	1
AL-Ch	33	66	1	0.50	79	11	7	1	2	1

DBDO, Dibenzodioxocin; CA, cinnamyl aldehyde.

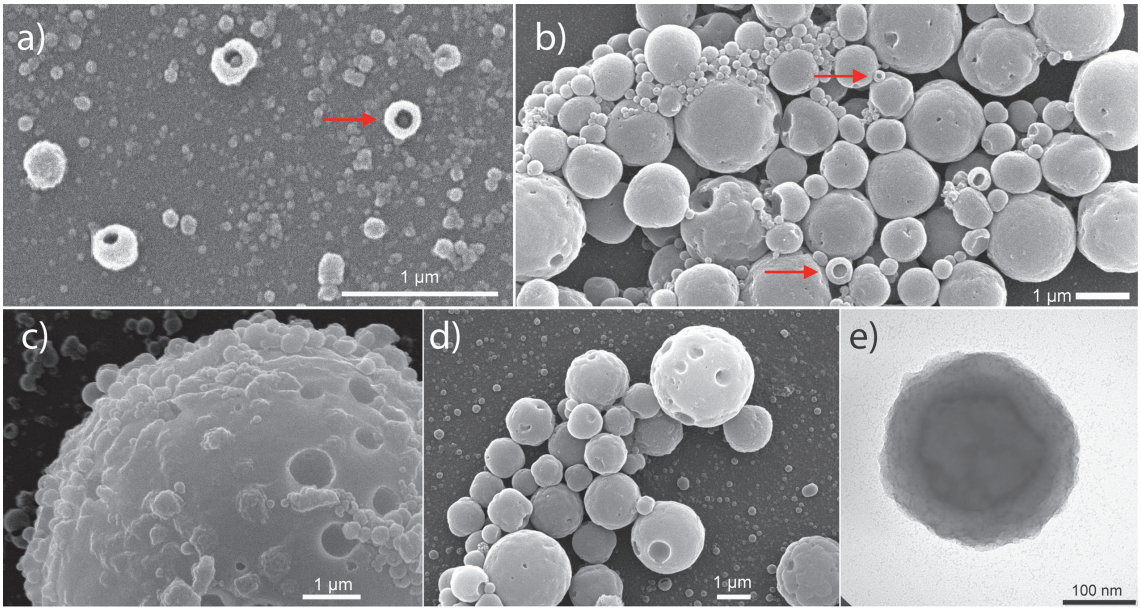

Figure 5: LNPs of different dimensional classes with diameters between 40 and 120 nm, as well as microparticles with diameters of several micrometers.
SEM (a–d) and TEM (e) micrographs of micro- and nanoparticles from beech acidolysis lignin.

a multimodal size distribution exhibiting a high-MM, medium-MM and low-MM maximum, whereas chestnut AL exhibited a uniform MMD with one maximum only (Figure 6a).

On the basis of the integrated peak areas in the pyrograms, the most relevant products of beech AL were syringol, 4-vinylsyringol, 4-propenylsyringol and syringaldehyde (peak numbers 7, 15, 21 and 22 in Figure 2 and Table 2). For chestnut, guaiacol, 4-methylguaiacol and 4-vinylguaiacol (peak numbers 1, 2 and 4) were predominant. The S/G ratios (Table 2) are conclusive, i.e. beech lignin is dominated by the S-type degradation products and chestnut lignin by the G-type degradation products. The S/G ratio of the isolated AL fractions is lower than in the original wood sample (OrigB and OrigCh), while the S/G ratios in acidolysis residues (ResB and ResCh) are higher in both cases (Table 2). S-type lignin is most abundant in the secondary cell wall, while G-units are predominant in the middle lamella (ML) and primary cell wall (Donaldson 2001). In view of milling to 35 mesh as the only pretreatment, it is reasonable that AL-B shows a lower S/G ratio than original beech wood, because a part of S-type lignin was probably not accessible by the isolation method applied here. The determined S/G ratio of AL-B is in good concordance with values reported by Genuit et al. (1987) obtained in a similar manner as in the present paper. The found S/G ratio was also corrected according to Choi et al. (2001), as it is well known that the S-type degradation products are overestimated in chemical degradation methods (Sarkanen and Hergert 1971) and also in analytical Py. (Genuit et al. 1987; Choi et al. 2001). The corrected values are also in agreement with the data reported by Choi et al. (2001) for different beech residual lignins. In Figure 2, the respective pyrograms of the original wood and acidolysis residual wood show abundant polysaccharide-type degradation products with retention times between 5 and 18 min (e.g. furfural at 9.22 min or γ-valerolacton at 13.67 min). Carbohydrate peaks with retention times below 19 min occurred in traces, and the levoglucosane peak (no. 20 in Figure 2) was small in the case of the AL fractions, which together with their KL content (Table 1) is indicative of a high purity.

Figure 3 shows the expanded aromatic and side-chain regions of the acquired 2D NMR spectra of AL-B and AL-Ch samples, respectively. The chemical shifts of the cross-peaks and the respective assigned chemical structures are listed in Table 3 and illustrated in Figure 4. For both AL-B and AL-Ch, the aromatic regions are dominated by cross-peaks of S and G units, while for H units only signal traces are detected. The estimated monomeric products and S/G ratios are listed in Table 4, which differ only by ≈10% from the respective uncorrected S/G ratios determined by analytical Py (Table 3). The agreement of the data sets obtained by two different approaches does not confirm the necessity to correct the overestimated S-type degradation products obtained by chemical or pyrolytical

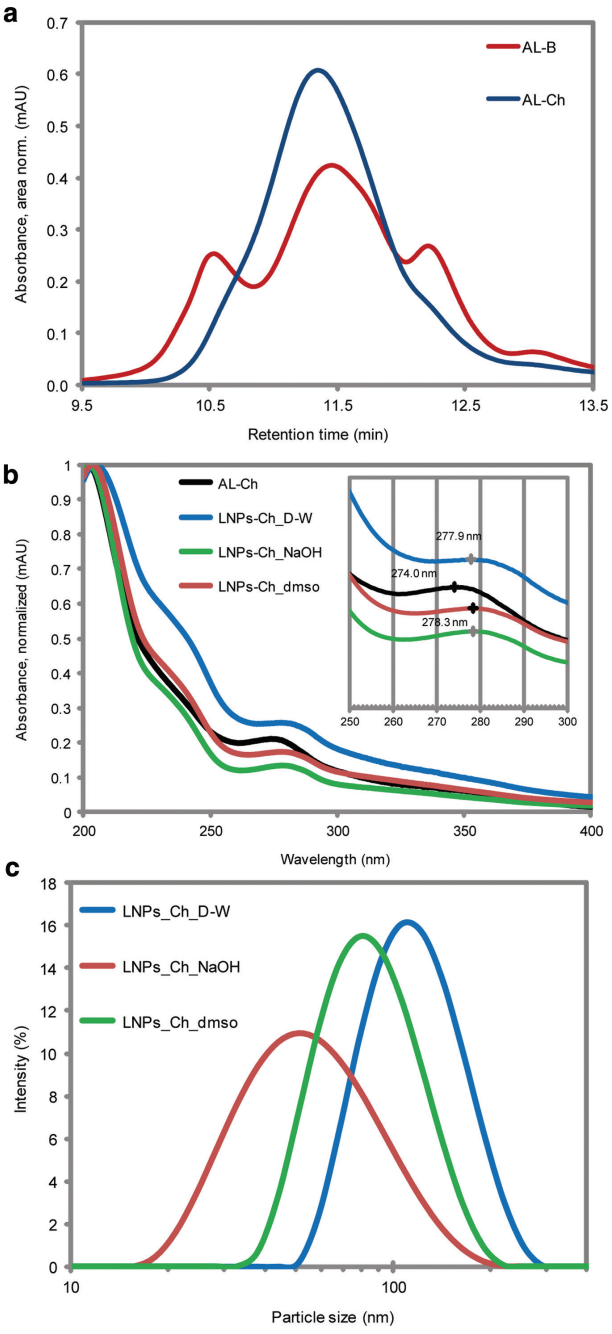

Figure 6: (a) Different molar mass distributions of the two isolated acidolysis lignin fractions from beech and chestnut (AL-B, AL-Ch). (b) LNPs-dispersions show UV absorption maxima shifts compared to the corrsponding acidolysis lignin UV spectrum. (c) DLS experiments result in different size distributions depending on the solvent used for the respective acidolysis lignin stock solution.
(a) Size exclusion chromatograms of beech and chestnut acidolysis lignins (AL-B, AL-Ch). (b) UV spectra of AL from chestnut (AL-Ch) and of the respective nanoparticle dispersions (LNPs-Ch_D-W, LNPs-Ch_NaOH, LNPs-Ch_dmso) made from the different stock solutions in dioxane/water, NaOH and DMSO. (c) DLS determination of the size distribution of chestnut LNP dispersions derived from the three different lignin stock solutions (see above).

degradation. Both AL fractions indicate the presence of β-O-4′-linkages in high amounts, thus the mild acidolysis seems to be well suited for lignin isolation leading to moderate changes in the native structure. Besides the main lignin linkages (β-O-4′-, β-5′-, and β-β′), signals for dibenzodioxocin (DBDO) and benzyl ether substructures were identified with low ratios of 1–2% (Table 4). AL-Ch samples show a higher ratio of β-5′ substructures, which is related to the higher content of G units with a free C_5 position on the aromatic ring. In the side-chain regions of the NMR spectra, xylan cross-peaks were identified, which correlates to the data listed in Table 1. Minor peaks of furfural in the carbohydrate region are in agreement with the observations on the pyrograms of AL-B and AL-Ch (Figure 2).

Lignin nanoparticles (LNPs)

SEM and TEM analyses show that the formed LNPs grouped up mainly within two dimensional classes with diameters between 40–50 and 100–120 nm (Figure 5a). Furthermore, particles with diameters around 0.45–1.0 µm and larger were detected, which have pores on their surface (Figure 5b and d). Moreover, agglomerates of nanoparticles were detected surrounding bigger microparticles with diameters >5 µm indicating that pores on the surface could act as nucleation sites for smaller particles (Figure 5c). In agreement with Xiong et al. (2017a), the SEM micrographs also indicate the presence of hollow particles, while some of them carry other particles inside their cavities (Figure 5a). In one specific case (Figure 5a, red arrow), the hollow particle had a diameter of 240 nm with a hole opening of 120 nm and contained another particle with an estimated diameter of 70 nm. Other examples (Figure 5b, red arrows) had a particle diameter of 500 nm and 220 nm with openings of 250 nm and 100 nm, respectively. The hollow shell character of the particles was confirmed by TEM experiments showing a dark area inside the particles void of material (Figure 5d). This observation is interpreted as that the produced nanoparticles could be loaded with bioactive molecules for controlled-release applications (Mattos et al. 2017). Bioremediation applications might also be conceivable, as pollutants can be readily adsorbed on the porous surface of LNPs or inside their cavities.

Comparison of the UV spectra of the chestnut AL fraction and the respective LNPs derived from the different stock solutions show a clear shift to a higher wavelength of $\lambda_{280\,nm}$ (Figure 6b). These findings are in agreement with

those reported by Xiong et al. (2017a), who argued that LNP formation is initialized through a so-called π-stacking, π-π-interactions between the aromatic rings, and found a red-shift of the lignin UV λ_{max} of the LNPs. A bathochromic shift in the UV spectra of LNPs from kraft lignin was also observed by Li et al. (2016), who attributed this to the increased π-π-aggregation of the nanosphere sample.

DLS experiments of pre-filtered (0.45 µm) LNP dispersions show particle size distributions with different maxima depending on the isolation parameters (Figure 6c). Obviously, there is a possibility to affect both size and frequency of LNP distribution by solvent selection in the course of fabrication.

The aqueous LNP dispersions were freeze-dried and submitted to FTIR spectroscopy (Figure 7). The high similarity between the lignin and LNP spectra is an indication of the little chemical changes between the samples. However, the intensities of the bands attributed to lignin aromatic ring breathing modes (1328 cm^{-1}, 1268 cm^{-1} and 1225 cm^{-1}) are relatively lower than those attributed to other aromatic skeletal vibration modes. This is probably due to abundant π-stacking of aromatic rings in LNPs leading to a reduction of their freedom for aromatic ring breathing. Furthermore, a new band was detected at 1385 cm^{-1} in both LNP fractions. Colom et al. (2003) attributed this to conformational changes in the β-glycosidic bond of cellulose due to disturbances in its chemical environment, which could be caused by lignin π-stacks in the close chemical environment of cellulose residues in the AL fractions.

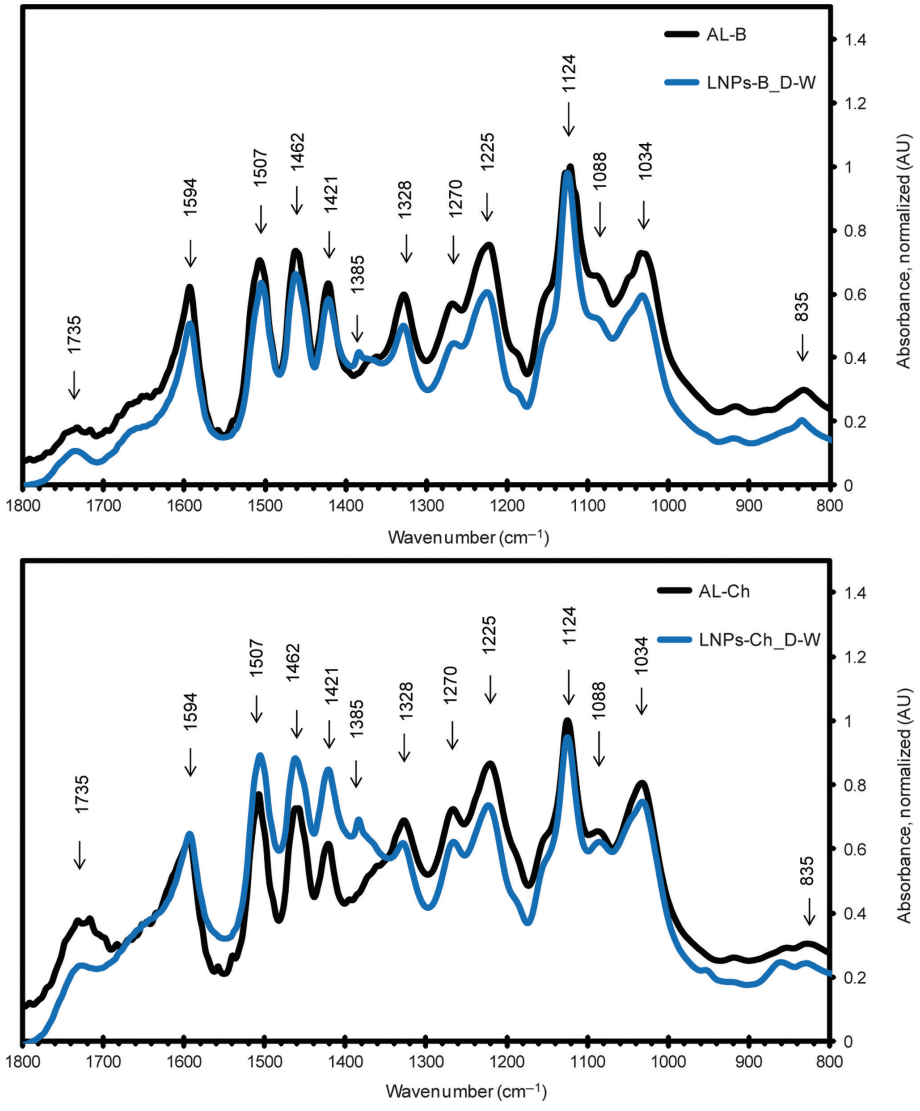

Figure 7: FTIR spectra of acidolysis lignin (AL) fractions from beech wood and chestnut sawdust (AL-B, AL-Ch) and freeze-dried lignin nanoparticles (LNPs) derived from the respective dioxane/water stock-solutions (LNPs-B_D-W, LNPs-Ch_D-W).

Conclusions

Lignin from residual wood and wood waste was isolated and converted to lignin microparticles and LNPs. Both beech and chestnut woods proved to be satisfying starting materials for LNP preparation, which show only moderate chemical changes compared to native lignin. Lignin microspheres with a high surface porosity as well as hollow nanospheres were observed in the fabricated aqueous dispersions, which are expected to offer a wide potential for controlled-release applications and environmental protection. The choice of the lignin solvent had a clear influence on the final LNPs' dimensions, i.e. the LNP properties can be controlled by solvent variation of the initial lignin stock solution. Solvents such as NaOH and DMSO were successfully tested for the preparation of LNPs.

Acknowledgments: This work was conducted in the frame of the PRIN-MIUR 2015 (Research Projects of National Interest by the Ministry of Education, University and Research of Italy) "Wood value-chain" project (grant number: 2015YW8JWA, coord. G. Scarascia-Mugnozza). Financial support from the PON R&C ALForLab (grant number: PON03PE_00024_1) Public-Private Partnership and the CNR-ISAFOM Institute (Dir. G. Matteucci) is also gratefully acknowledged. Support with 2D HSQC NMR spectroscopy experiments from Prof. Roberta Bernini from the Department of Agricultural and Forestry Sciences (DAFNE), University of Tuscia, Viterbo, Italy, is gratefully acknowledged. Support in dynamic light scattering experiments from Nathalie Sandrine Bieri from Bern University of Applied Sciences, Wood and Civil Engineering, area of competence Materials and Wood Chemistry, is gratefully acknowledged.

Author contributions: All the authors have accepted responsibility for the entire content of this submitted manuscript and approved submission.
Research funding: None declared.
Employment or leadership: None declared.
Honorarium: None declared.

References

Ago, M., Tardy, B.L., Wang, L., Guo, J., Khakalo, A., Rojas, O.J. (2017) Supramolecular assemblies of lignin into nano- and microparticles. MRS Bull. 42:371–378.

Beisl, S., Miltner, A., Friedl, A. (2017) Lignin from micro- to nanosize: production methods. Int. J. Molec. Sci. 18:1244.

Chen, T.-Y., Wang, B., Shen, X.-J., Li, H.-Y., Wu, Y.-Y., Wen, J.-L., Liu, Q.-Y., Sun, R.-C. (2017) Assessment of structural characteristics of regenerated cellulolytic enzyme lignin based on a mild DMSO/[Emim]OAc dissolution system from triploid of *Populus tomentosa* Carr. RSC Adv. 7:3376–3387.

Choi, J.W., Faix, O., Meier, D. (2001) Characterization of residual lignins from chemical pulps of spruce (*Picea abies* L.) and beech (*Fagus sylvatica* L.) by analytical pyrolysis-gas chromatography/mass spectrometry. Holzforschung 55:185–192.

Colom, X., Carrillo, F., Nogués, F., Garriga, P. (2003) Structural analysis of photodegraded wood by means of FTIR spectroscopy. Polym. Degrad. Stabil. 80:543–549.

Conedera, M., Tinner, W., Krebs, P., de Rigo, D., Caudullo, G. (2016) *Castanea sativa* in Europe: distribution, habitat, usage and threats. In: European Atlas of Forest Tree Species. Eds. San-Miguel-Ayanz, J., de Rigo, D., Caudullo, G., Houston Durrant, T., Mauri, A. Publ. Off. EU, Luxembourg. pp. 78–79.

Donaldson, L.A. (2001) Lignification and lignin topochemistry – an ultrastructural view. Phytochemistry 57:859–873.

Faix, O. (1991) Classification of lignins from different botanical origins by FT-IR spectroscopy. Holzforschung 45(Supplement, September):21–27.

Faix, O. (1992) Fourier transform infrared spectroscopy. In: Methods in Lignin Chemistry. Eds. Lin, S.Y., Dence, C.W. Springer Berlin Heidelberg, Berlin, Heidelberg. pp. 233–241.

Faix, O., Meier, D., Fortmann, I. (1990a) Thermal degradation products of wood: a collection of electron-impact (EI) mass spectra of monomeric lignin derived products. Holz Roh. Werkst. 48:351–354.

Faix, O., Meier, D., Fortmann, I. (1990b) Thermal degradation products of wood: gas chromatographic separation and mass spectrometric characterization of monomeric lignin derived products. Holz Roh. Werkst. 48:281–285.

Faix, O., Fortmann, I., Bremer, J., Meier, D. (1991a) Thermal degradation products of wood: a collection of electron-impact (EI) mass spectra of polysaccharide derived products. Holz Roh. Werkst. 49:299–304.

Faix, O., Fortmann, I., Bremer, J., Meier, D. (1991b) Thermal degradation products of wood: gas chromatographic separation and mass spectrometric characterization of polysaccharide derived products. Holz Roh. Werkst. 49:213–219.

Fortunati, E., Yang, W., Luzi, F., Kenny, J., Torre, L., Puglia, D. (2016) Lignocellulosic nanostructures as reinforcement in extruded and solvent casted polymeric nanocomposites: an overview. Eur. Polym. J. 80:295–316.

Frangville, C., Rutkevicius, M., Richter, A.P., Velev, O.D., Stoyanov, S.D., Paunov, V.N. (2012) Fabrication of environmentally biodegradable lignin nanoparticles. Chemphyschem 13:4235–4243.

Gellerstedt, G., Pranda, J., Lindfors, E.L. (1994) Structural and molecular properties of residual birch kraft lignins. J. Wood Chem. Techn. 14:467–482.

Genuit, W., Boon, J.J., Faix, O. (1987) Characterization of beech milled wood lignin by pyrolysis-gas chromatography-photoionization mass spectrometry. Anal. Chem. 59:508–513.

Houston Durrant, T., de Rigo, D., Caudullo, G. (2016) *Fagus sylvatica* and other beeches in Europe: distribution, habitat, usage and threats. In: European Atlas of Forest Tree Species. Eds. San-Miguel-Ayanz, J., de Rigo, D., Caudullo, G., Houston Durrant, T., Mauri, A. Publ. Off. EU, Luxembourg. pp. 94–95.

Kim, H., Ralph, J. (2010) Solution-state 2D NMR of ball-milled plant cell wall gels in DMSO-d6/pyridine-d5. Org. Biomol. Chem. 8:576–591.

Li, H., Deng, Y., Wu, H., Ren, Y., Qiu, X., Zheng, D., Li, C. (2016) Self-assembly of kraft lignin into nanospheres in dioxane-water mixtures. Holzforschung 70:725–731.

Lievonen, M., Valle-Delgado, J.J., Mattinen, M.-L., Hult, E.-L., Lintinen, K., Kostiainen, M.A., Paananen, A., Szilvay, G.R., Setälä, H., Österberg, M. (2016) A simple process for lignin nanoparticle preparation. Green Chem. 18:1416–1422.

Lourenço, A., Rencoret, J., Chemetova, C., Gominho, J., Gutiérrez, A., del Río, J.C., Pereira, H. (2016) Lignin composition and structure differs between xylem, phloem and phellem in *Quercus suber* L. Front. Plant Sci. 7:1612.

Mattos, B.D., Tardy, B.L., Magalhães, W.L.E., Rojas, O.J. (2017) Controlled release for crop and wood protection: recent progress toward sustainable and safe nanostructured biocidal systems. J. Control. Release 262:139–150.

Mattsson, T., Azhar, S., Eriksson, S., Helander, M., Henriksson, G., Jedvert, K., Lawoko, M., Lindström, M.E., McKee, L.S., Oinonen, P., Sevastyanova, O., Westerberg, N., Theliander, H. (2017) The development of a wood-based materials-biorefinery. BioResources 12:9152–9182.

Moghaddam, L., Rencoret, J., Maliger, V.R., Rackemann, D.W., Harrison, M.D., Gutiérrez, A., del Río, J.C., Doherty, W.O.S. (2017) Structural characteristics of bagasse furfural residue and its lignin component. An NMR, Py-GC/MS, and FTIR study. ACS Sustain. Chem. Eng. 5:4846–4855.

Nalaparaju, A., Jiang, J. (2012) Recovery of dimethyl sulfoxide from aqueous solutions by highly selective adsorption in hydrophobic metal–organic frameworks. Langmuir 28:15305–15312.

Paletto, A., Giacovelli, G., Matteucci, G., Maesano, M., Pastorella, F., Turco, R., Scarascia Mugnozza, G. (2017) Strategies for the promotion of the forest-wood chain in Calabria (southern Italy): the stakeholders' point of view. Forest@ 14:34–48.

Ragauskas, A.J., Beckham, G.T., Biddy, M.J., Chandra, R., Chen, F., Davis, M.F., Davison, B.H., Dixon, R.A., Gilna, P., Keller, M., Langan, P., Naskar, A.K., Saddler, J.N., Tschaplinski, T.J., Tuskan, G.A., Wyman, C.E. (2014) Lignin valorization: improving lignin processing in the biorefinery. Science 344:1246843.

Ralph, S.A., Ralph, J., Landucci, L.L. (2009) NMR Database of Lignin and Cell Wall Model Compounds. Available at URL http://www.glbrc.org/databases_and_software/nmrdatabase/ (accessed Feb 10, 2018).

Russo, D., Macrì, G., Luzzi, G., De Rossi, A. (2016) Wood energy plants and biomass supply chain in Southern Italy. Procedia Soc. Behav. Sci. 223:849–856.

Sarkanen, K.V., Hergert, H.L. (1971) Classification and distribution. In: Lignins – Occurrence, Formation, Structure and Reactions. Eds. Sarkanen, K.V., Ludwig, C.H. Wiley-Interscience, New York. pp. 43–94.

Sundergopal, S., Cheekapally, P.R., Yerrapragada, V.L.R., Kunduvelil, S.M.R., Mannava, G.C.R., Kammara, S., Boinee, V. (2011) Electrodialysis-distillation hybrid process for the recovery of dimethylsulfoxide (DMSO) solvent from industrial effluent. World patent WO2011055381A1. Available at: https://patents.google.com/patent/WO2011055381A1/en.

TAPPI T 222. om-02, Acid-insoluble lignin in wood and pulp, 2002–2003 Tappi Test Methods. Tappi Press, Atlanta, GA, USA.

Traoré, M., Kaal, J., Martínez Cortizas, A. (2016) Application of FTIR spectroscopy to the characterization of archeological wood. Spectrochi. Acta A 153:63–70.

Tuck, C.O., Perez, E., Horvath, I.T., Sheldon, R.A., Poliakoff, M. (2012) Valorization of biomass: deriving more value from waste. Science 337:695–699.

Van Soest, P.J. (1963) Use of detergents in the analysis of fibrous feeds. II. A rapid method for the determination of fiber and lignin. J. Assoc. Off. Ana. Chem. 46:829–835.

Van Soest, P.J., Wine, R.H. (1967) Use of detergents in the analysis of fibrous feeds. IV. Determination of plant cell-wall constituents. J. Assoc. Off. Ana. Chem. 50:50–55.

Xiong, F., Han, Y., Wang, S., Li, G., Qin, T., Chen, Y., Chu, F. (2017a) Preparation and formation mechanism of renewable lignin hollow nanospheres with a single hole by self-assembly. ACS Sustain. Chem. Eng. 5:2273–2281.

Xiong, F., Han, Y., Wang, S., Li, G., Qin, T., Chen, Y., Chu, F. (2017b) Preparation and formation mechanism of size-controlled lignin nanospheres by self-assembly. Ind. Crop. Prod. 100:146–152.

Zajáros, A., Matolcsy, K. (2016) DMSO contaminated industrial wastewater recycling by distillation, 3rd International Congress on Water, Waste and Energy Management, Rome.

Zikeli, F., Ters, T., Fackler, K., Srebotnik, E., Li, J. (2014) Successive and quantitative fractionation and extensive structural characterization of lignin from wheat straw. Ind. Crop. Prod. 61:249–257.

Zikeli, F., Ters, T., Fackler, K., Srebotnik, E., Li, J. (2016) Wheat straw lignin fractionation and characterization as lignin-carbohydrate complexes. Ind. Crop. Prod. 85:309–317.